frontiers in Earth Science

ORIGINAL RESEARCH
published: 15 April 2021
doi: 10.3389/feart.2021.634354

# Multi-Proxy Records of Late Holocene Flood Events From the Lower Reaches of the Narmada River, Western India

*Prabhin Sukumaran[1], Dhananjay A. Sant[2]*, K. Krishnan[3], Govindan Rangarajan[4], Nathani Basavaiah[5] and Jean-Luc Schwenninger[6]*

*[1] Department of Civil Engineering, Chandubhai S. Patel Institute of Technology, Charotar University of Science and Technology, Changa, India, [2] Department of Geology, Faculty of Science, The Maharaja Sayajirao University of Baroda, Vadodara, India, [3] Department of Archaeology and Ancient History, Faculty of Arts, The Maharaja Sayajirao University of Baroda, Vadodara, India, [4] Department of Mathematics, Indian Institute of Science, Bengaluru, India, [5] Indian Institute of Geomagnetism, Mumbai, India, [6] Research Laboratory for Archaeology and the History of Art, School of Archaeology, University of Oxford, Oxford, United Kingdom*

OPEN ACCESS

**Edited by:**
*Joyanto Routh, Linköping University, Sweden*

**Reviewed by:**
*Manoj Jaiswal, Indian Institute of Science Education and Research Kolkata, India*
*Lisa Ely, Central Washington University, United States*

***Correspondence:**
*Dhananjay A. Sant*
*sant.dhananjay-geology@msubaroda.ac.in*

**Specialty section:**
*This article was submitted to Quaternary Science, Geomorphology and Paleoenvironment, a section of the journal Frontiers in Earth Science*

**Received:** *27 November 2020*
**Accepted:** *22 March 2021*
**Published:** *15 April 2021*

**Citation:**
*Sukumaran P, Sant DA, Krishnan K, Rangarajan G, Basavaiah N and Schwenninger J-L (2021) Multi-Proxy Records of Late Holocene Flood Events From the Lower Reaches of the Narmada River, Western India. Front. Earth Sci. 9:634354. doi: 10.3389/feart.2021.634354*

Analyses of a fluvial sedimentary sequence from the lower reaches of the Narmada River establish a record of rhythmic cycles of sediment facies that represent floods during the late Holocene. The south-west Indian monsoon strongly influences the study area, and heavy rainfall or cyclones which originate from either the Bay of Bengal or the Arabian Sea, also affect the region. Optically stimulated luminescence dating places the 8 m thick sediment sequence in the climate transition phase which ranges from the Medieval Warm Period to the Little Ice Age. Multi-proxy analyses including high-resolution granulometry, magnetic susceptibility, ferromagnetic mineral concentration, facies major oxide geochemistry, and micro-fossil records (from two sedimentary units) are used to study these late Holocene flood events. The latter are characterised by multiple sediment facies, depositional events, changes in channel morphology, and distinctive flood signatures. Integration of these records enables to identify two distinct aggradations viz. phase I and phase II, as well as a relative change in channel morphology. The study describes 11 flooding events and their imprints over multi-proxy records. Historic documents and instrumental records from the town of Bharuch referring to floods, movement of channel sand, channel shallowing, and the dysfunction of the ancient port of Bharuch further validate the inferences drawn from the sedimentary sequence. The study exemplifies the need to use high resolution and multi-proxy studies to interpret paleoflood records and climate signatures in order to build archives of monsoonal rivers.

**Keywords: Little Ice Age, southwest Indian monsoon, flood events, magnetic susceptibility, ferromagnetic mineral concentration, geochemistry**

**Abbreviations:** LIA, Little Ice Age; MWP, Medieval Warm Period; SwIM, Southwest Indian Monsoon; LrNR, Lower reaches of Narmada River; OSL, Optically Stimulated Luminescence; MS, Magnetic susceptibility; FMC, Ferrimagnetic Mineral Concentration; CIA, Chemical Index of Alteration; AP I, Aggradation Phase I and AP II, Aggradation Phase II; MSD, Monsoonal Storm Deposits.

## INTRODUCTION

Globally, river terrace sequences are widely recognised as sources for understanding Quaternary paleo-environments over the continent (Gao et al., 2016; Kolb et al., 2016; Stanford et al., 2016; Sun et al., 2016; Vázquez et al., 2016). In India, several studies have revealed that the sedimentary sequences along monsoonal rivers are not different, and preserve Quaternary flood events (**Table 1**). The Narmada River is one of the most significant, westerly flowing rivers that emerges from the Maikala Range (1,057 m a.s.l) of the Amarkantak Plateau in Central India (**Figure 1**). It flows into the Gulf of Cambay in the Arabian Sea about 50 km west of the town of Bharuch. The Narmada River's flood-prone character is substantiated by the consistent presence of a low-pressure track along the Narmada River valley during the monsoonal months (June–September). During these months, the low-pressure track steers the moisture-laden clouds (tropical storms) toward the northwest and north after gathering over the Bay of Bengal and the Arabian Sea, respectively, which regulate the distribution of rainfall, and thereby the floods over the Indian subcontinent. The river terrace sediments from the lower Narmada River valley may be considered a reliable proxy for monsoonal floods, assuming they can be systematically decoded.

The drainage basin of the lower reaches of the Narmada River (LrNR) exposes five distinct lithological terrains, namely, Proterozoic crystalline rocks (Lunavada Group, Champaner Group, and Godhra granite), Cretaceous infra-trappeans (Bagh Group and Lameta Formation), Deccan Trap, Tertiary sediments and Quaternary valley-fill deposits (**Figure 1-III**). The Orsang River forms the major tributary of the Narmada River on the northern bank. It covers a broad catchment over crystalline rocks exposed in the north-western Narmada Basin. The silica sand that fills the present-day channel is brought into the Narmada channel through the Orsang River. The Narmada River and the Karjan River (a major southern bank tributary of the Narmada River), both emerge from the Deccan Trap terrain and remain a significant sediment source other than silica sand.

Geomorphologically, the LrNR draws attention to three prominent landforms, namely, relic alluvial fans, paleo-banks, and neo-banks (**Figure 1-IV**). Each of these landforms is characterised by distinctive litho-units (Bedi and Vaidyanadhan, 1982; Sant and Karanth, 1993; Sridhar and Chamyal, 2010; Sukumaran et al., 2012a,b; Sridhar et al., 2015). The minimum age of these landforms is estimated from the chronology of the sedimentary sequence with alluvial fans dating to the early late Pleistocene (∼90 ka: Chamyal et al., 2002; Joshi et al., 2013), paleo-bank deposits dating to the middle-late Pleistocene (∼24.5–74 ka; Chamyal et al., 2002; Raj, 2008) and neo-bank sedimentary units dating to the late Holocene (Raj and Yadava, 2009; Sridhar et al., 2015).

The present study examines neo-bank sequences that preserve historic flood imprints and help to understand changes in the southwest Indian monsoon (SwIM) dynamics. A high-resolution, multi-proxy fluvial record from the site of Uchediya (21°43′ 2.22″ N, 73° 6′ 26.22″ E) located 10 m a.s.l in the core portion of "the neo-bank" is the focus of this study. This landform has laterally aggraded for about 45 km (from the village of Rajpardi in the east to the village of Hansot in the west) within the southern Narmada paleo-bank (**Figure 1-IV**). The high-resolution granulometric data and micropaleontological findings for the Uchediya site have been discussed previously (Sukumaran et al., 2012a,b). In the present study, we further integrate available findings on granulometric and micropaleontological data with three new dates obtained by optically stimulated luminescence (OSL) as well as high-resolution magnetic susceptibility (MS), ferromagnetic mineral concentration (FMC) and facies representative major oxide geochemistry (FMoG). Our findings lead us to propose an aggradation model with the sequence of change in the channel morphology corresponding to late Holocene climate and flood events.

## METHODS AND RESULTS

### Chronology of the Uchediya Sequence

Samples for optically stimulated luminescence (OSL) dating (Aitken, 1998) were collected in steel tubes at regular 50 cm intervals along the exposed section whilst taking good care to avoid accidental exposure to sunlight (**Figure 2**). Following detailed sedimentological studies, three samples (X3543, X3544, and X3545) taken from 50, 200, and 800 cm below the modern surface were selected for analysis to bracket the landform's primary aggradation time frame. Sample preparation and measurements were conducted at the luminescence dating laboratory of the Research Laboratory for Archaeology and the History of Art, University of Oxford. Sample preparation took place under low-intensity safe-lighting provided by filtered sodium lamps (emitting at 588 nm). Standard laboratory preparation techniques were applied to yield sand-sized (180–255 μm) grains of quartz for optical dating. These included wet sieving, HCl (10%) treatment to remove carbonates, 30% $H_2O_2$ treatment to remove organic matter and HF (68%) etching to remove the outer (∼10 mic) rind of quartz grains affected by alpha irradiation and to dissolve feldspathic minerals. Heavy minerals were removed by density gradient separation using a liquid solution of sodium polytungstate (delta = 2.65 gcm $^{-3}$) followed by renewed rinsing in HCl (10%) to eliminate potential fluorite contaminants with a final cleaning in demineralised water. Dried quartz grains were then mounted onto aluminium discs as small (diam. = 2 mm) multigrain ($n$ = 50–100 grains) aliquots using a silicon oil adhesive (Viscasil 60,000).

OSL measurements were conducted using an automated Risø TL/OSL-DA-15 luminescence reader (Bøtter-Jensen, 1997) and are based on a conventional single-aliquot regeneration (SAR) measurement protocol (Murray and Wintle, 2000). Repeat palaeodose measurements were made for each sample ($n$ = 18 or 28), and optical stimulation was provided by blue light-emitting diodes (42 Nichia 470Δ20 nm; 36 mW cm$^{-2}$). Given the young age of the sediment, the natural and regenerative doses were preheated at a relatively low temperature of 200°C for 10 s and the fixed test doses (which are used to correct for any sensitivity changes) were preheated at a reduced temperature of 180°C for 10 s, before optical stimulation. In order to minimise the contribution of residual feldspathic components

**TABLE 1 |** Various flood sequence sites studied along monsoonal rivers across the Indian subcontinent.

| Sr No | Site | River | Landform | Max age | Min age | No. of flood events | References |
|---|---|---|---|---|---|---|---|
| 1. | Sakarghat | Central Narmada | Terrace within George | 1923 ± 86*BP* | 690 ± 45*BP* | 26 | Kale et al., 1997b |
| 2. | Bhuka | Luni | Terrace within George | 990 ± 130*BP* | 540 ± 80*BP* | 21 | Kale and Baker, 2006 |
| 3. | Guttigarh, | Tapi Upland | Terrace within George | 240 ± 50*BP* | 156 ± 52*BP* | 4–5 | Kale et al., 2003 |
| 4. | Teska | Tapi Upland | Terrace within George | 225 ± 40*BP* | Post-1950 | 6–9 | Kale et al., 2003 |
| 5. | Khapa | Tapi Upland | Terrace within George | 380 ± 45*BP* | Younger | 13 | Kale et al., 2003 |
| 6. | Chahin Nala | Central Narmada | Terrace within George | Older | 1720 ± 185*BP* | 4 | Ely et al., 1996 |
| 7. | Chahin Nala | Central Narmada | Terrace within George | 1720 ± 185*BP* | 650 ± 70*BP* | 5 | Ely et al., 1996 |
| 8. | Dhamnacha | Lower Narmada | Terrace | 1350 ± 80*BP* | 360 ± 65*BP* | – | Sridhar et al., 2016 |
| 9. | Ranipura | Lower Narmada | Terrace | 2230 ± 90*BP* | 1010 ± 80*BP* | – | Sridhar et al., 2015 |
| 10. | Srisailam | Krishna | Terrace within George | 1690 ± 50*BP* | 1025 ± 55*BP* | 58 | Kale and Baker, 2006 |
| 11. | Kodepudi | Godavari River | Terrace within George | 2108 ± 58*BP* | 780 ± 60*BP* | ∼24 | Kale and Baker, 2006 |
| 12. | Racherla | Penner | Abandoned channel, Paleoflood and Pond deposits | 2860 ± 310*BP*(*OSL*) | 90 ± 15*BP*(*OSL*) | – | Thomas et al., 2007 |
| 13. | Punasa | Central Narmada | Terrace within George | 1450 ± 80*BP* | 445 ± 60*BP* | – | Baker, 1995 |
| 14. | Siddapur | Kaveri Upland | Terrace | 7900 ± 700(*OSL*) | 1700 ± 200(*OSL*) | ∼6 | Kale et al., 2010 |
| 15. | Timbi lake | Dhadhar | Lake deposits | 4220 ± 30*BP* | 250 ± 30*BP* | – | Sridhar et al., 2020 |
| 16. | Uchediya | Lower Narmada | Regional Terrace | 565 ± 60*Years* | 195 ± 25*Years* | 2-AP I 11-AP II | Present study |

to the quartz signal, each OSL measurement was proceeded by an infrared bleach at 50°C for 25 s before blue-light stimulation (Banerjee et al., 2001). The ultraviolet OSL emission of quartz at ∼370 nm was detected using an Electron Tubes Ltd 9235QA photomultiplier tube fitted with a blue-green sensitive bialkali photocathode and 7.5 mm of Hoya U-340 glass filter. Laboratory doses used for constructing dose-response curves were given using the $^{90}Sr/^{90}Y$ beta source housed within the reader. This source was calibrated against a gamma irradiated quartz standard supplied by Risø (Hansen et al., 2015).

The recorded OSL data were analysed with the "*Analyst*" software developed by Duller (2015), and a weighted mean equivalent dose (De) was calculated using the "*Luminescence*" package developed by Kreutzer et al. (2012) for the statistical programming language "*R*." The concentrations of radioactive elements (potassium, rubidium, thorium, and uranium) were determined by elemental analysis using ICP-MS/AES and converted to dose rates and luminescence age estimates using the conversion factors of Guérin et al. (2011) and the "*DRAC*" software developed by Durcan et al. (2015). The contribution of cosmic radiation to the total dose rate was calculated as a function of latitude, altitude and burial depth based on data by Prescott and Hutton (1994) and assuming an average overburden density of 1.9 $gcm^{-3}$. The sediment's recorded moisture content was found to be very low, with the upper sample containing only 3% water and the deeper samples X3544 and X3545, both providing even lower values around 1%. These measurements are not considered to be reliable, and the sediment almost certainly lost its pore water during the long 2 year storage period before the samples were sent for analysis. Therefore, the dose rate calculations are based on a more realistic estimated mean water content of 6% for sample X3543, 8% for X3544 and 10% for the basal sample X3545. A relatively large error of ± 5% was attached to each value to further compensate for this uncertainty, including likely seasonal variations in the sediment's uptake of water.

The paleodose (De) was determined by integrating the counts from the first second of the OSL decay curve, using the final 5 s as background noise. Dose response curves were fitted using a double saturating exponential function and are based on the weighted mean value derived from individual multigrain OSL measurements. A systematic laboratory reproducibility uncertainty of four per cent was added to each De measurement error to account for uncertainties in the calibration of the beta source. The majority of aliquots displayed high sensitivity, and the decay curves typically show a fast decreasing OSL signal. Measurements also showed a well-defined 110°C TL peak which is characteristic of quartz. Few aliquots revealed a noticeable response to infrared light stimulation, thereby confirming that good sample preparation had been achieved and/or relative sparseness of feldspathic components. Repeat measurements of the luminescence signal resulting from the first regeneration dose (recycling test) indicate that the adopted SAR procedure provides adequate correction for sensitivity changes with the mean value being close to unity (1.03). The same is also valid for recuperation which is generally below 3% as monitored by the OSL response after a regeneration dose of zero. A dose recovery test using the same preheat and measurement procedures as outlined above, was also performed on two aliquots from each sample (total $n = 6$). For this, mineral grains were first bleached in daylight for 3 h before they were given a small laboratory dose equivalent to 0.67Gy. The recovered mean dose for all six aliquots was 0.68 Gy (within 3%), thus confirming the suitability of the adopted measurement procedures. OSL age estimates are shown in **Table 2** alongside the radioactivity data and are based on a weighted mean. Kernel density plots

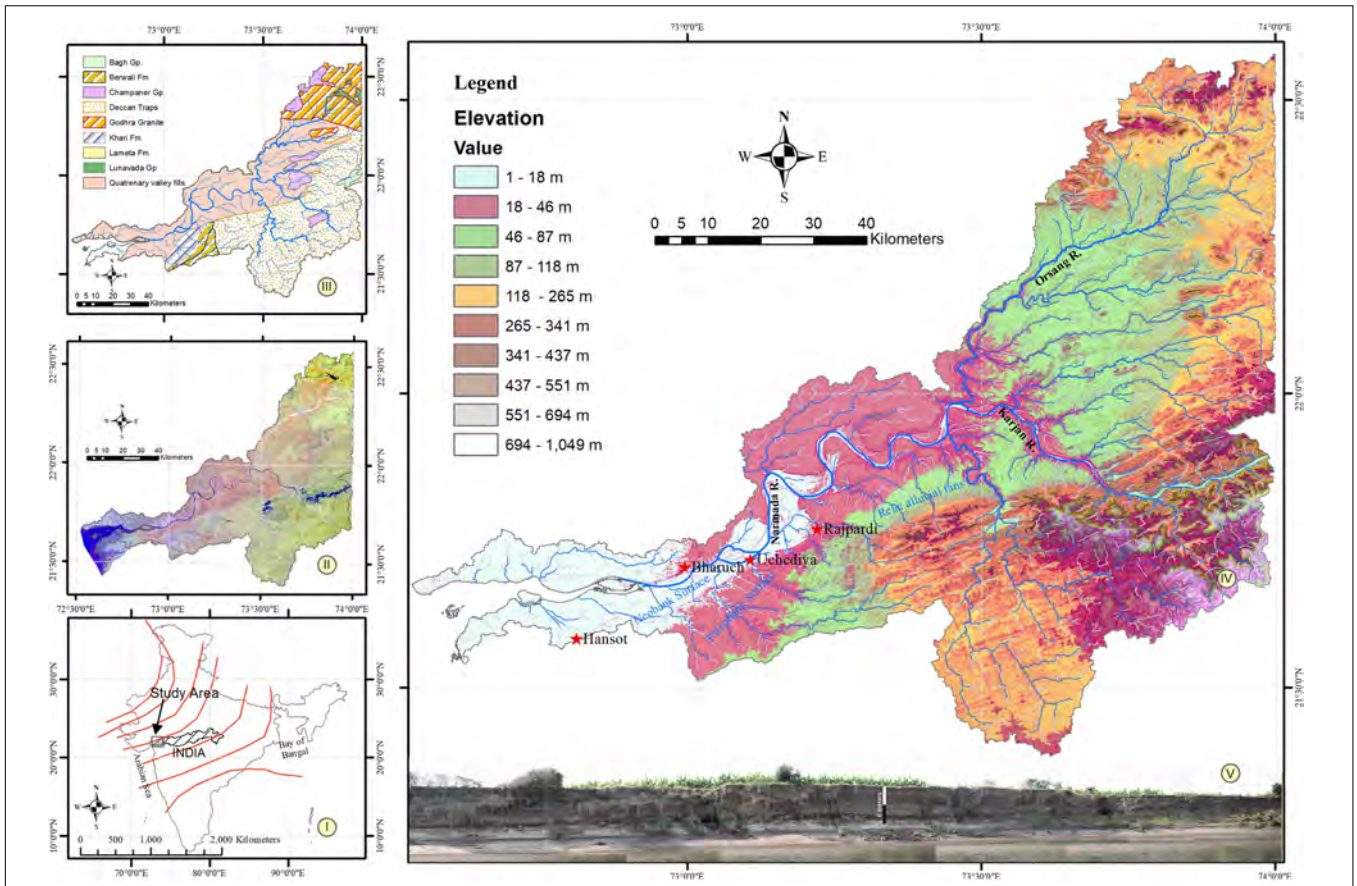


**FIGURE 1 | (I)** Index map of the study area showing normal withdrawal track (source: Indian Meteorological Department) of SW Indian monsoon **(II)** Landsat 8, false colour compost map of the study area with band composites Band 5 (NIR), Band 6 (SWIR-1) and Band 2 (Blue). **(III)** Geological map of the study area modified after the Geological Survey of India Geological map (https://bhukosh.gsi.gov.in/Bhukosh/MapViewer.aspx). **(IV)** Geomorphological map of the study area. Locations of important places mentioned in the text are marked. The neobank surface is bounded within the elevation of 1–18 m and the paleo-bank surface is bound between 18 and 46 m. Above 46 m the topography is produced by relict fanglomerates and upland rocks. **(V)** A regional view of the neobank sequence.

featuring the distribution of individual De values for each sample are presented in **Figure 3**, along with additional statistical information. Despite their fluvial nature, neither of the three samples was considered to suffer from partial bleaching and provided acceptable overdispersion levels ranging from 16 to 45%. Four high outlier values were identified among the 28 aliquots measured for sample X3545, and these were removed from the calculation of the weighted mean paleodose.

Sample X3543 collected from a depth of 50 cm provided an age of 195 ± 25 years, sample X3544 from a depth of 200 cm provided an age of 625 ± 45 years, and sample X3545 from a depth of 800 cm (base of the sequence) provided an age of 565 ± 60 years. Sample X3544 was collected from the interface of two sub-facies in the sediment sequence. This age estimate could be an overestimation of the actual age because the sample was collected from the boundary of coarser and finer sediment sub-facies. In the absence of *in situ* radioactivity measurements with a calibrated gamma-ray spectrometer, it is impossible to correctly assess the external gamma dose contribution to the total dose received by this sample. However, to evaluate the assumption further, we also considered a 50% contribution to the external gamma dose rate from the overlying fine sediment facies (X3543) for the age calculation of X3544. The resultant revised age estimate would be 550 ± 50 years, and this result would be in better agreement with the date of 565 ± 60 years obtained for the underlying basal sample X3545.

The OSL dating results strongly suggest that the bulk of the sediment at the base of the section (from 200 to 800 cm) was deposited within a relatively short period of time. In contrast, the overlaying 200 cm comprising finer facies took around 500 years. A relative maximum age determined using $^{14}C$ dating on a sequence from the same landform upstream of the Uchediya range dates from 1010 ± 60 to 2230 ± 90 years BP (Sridhar et al., 2015). With the above understanding, the sediment sequence is bracketed between 565 ± 60 years before 2020, i.e., 1395–1515 AD at a depth of 800 cm to 195 ± 25 years before 2020, i.e., 1800–1850 AD at a depth of 50 cm.

## High-Resolution Granulometric Records

Sediment samples were collected from a cut open trench of the present-day river bank (**Figure 2**). All 401 samples were collected

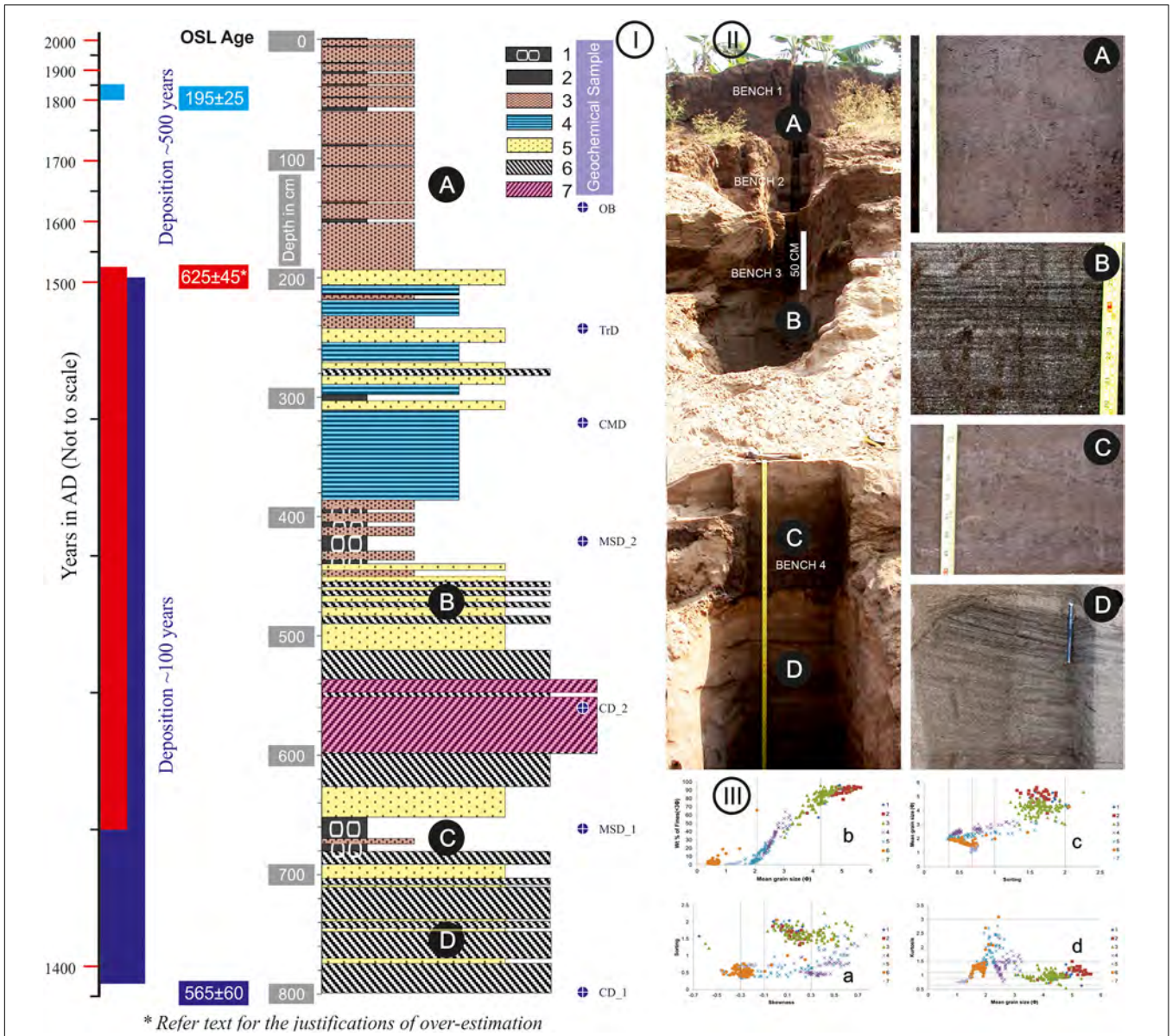


**FIGURE 2 |** Details of Uchediya sequence modified after Sukumaran et al. (2012b) summarising different characteristics of the Uchediya sequence **(I)** Change in sediment facies along depth profile (1, $Fm_{SILT+VFS}$ (T); 2, $Fm_{SILT+VFS}$ (O); 3, $Fm_{SILT+VFS+FS}$; 4, $Sl_{FS+VFS}$; 5, $Sm_{FS+MS}$; 6, $St_{MS+FS+CS}$; 7, $St_{MS+CS}$). CD-Channel deposit; MSD-monsoonal storms deposits; CMD-Channel margin deposits; TrD-Transition deposit; OB-Overbank deposits. **(II)** Filed photograph of a cut-open trench of the Uchediya sequence. **(A–D)** are photographs of different sub-facies. **(III)** Bivariate plots of different granulometric parameters.

**TABLE 2 |** Summary of OSL dating and radioactivity data.

| Lab. code | Field code | Depth (cm) | Water (%) | K (%) | Th (ppm) | U (ppm) | External (Gy/ka) | Cosmic (Gy/ka) | Total dose rate (Gy/ka) | Number aliquots | De (Gy) | OSL age[b] (years) |
|---|---|---|---|---|---|---|---|---|---|---|---|---|
| X3543 | DUCH1 | 50 | 6±5 | 1.00 | 10.3 | 1.9 | 0.955±0.06 | 0.19±0.02 | 2.18±0.12 | 18 | 0.43±0.05 | 195±25 |
| X3544 | DUCH4 | 200 | 8±5 | 1.27 | 5.9 | 1.1 | 0.722±0.04 | 0.15±0.05 | *1.89±0.12* | 28 | 1.18±0.04 | *625±45* |
| X3545 | DUCH16 | 800 | 10±5 | 1.26 | 2.8 | 0.7 | 0.526±0.04 | 0.08±0.01 | 1.50±0.11 | 28 | 0.85±0.06 | 565±60 |

[a] *Measurements were made on dried, homogenised and powdered material by ICP-MS/AES with an assigned systematic uncertainty of ± 10%. Dry beta and gamma dose rates were calculated from these activities and were adjusted for the estimated field water content.*
[b] *The age datum refers to AD 2020 and the luminescence dates are based on a weighted mean palaeodose.*

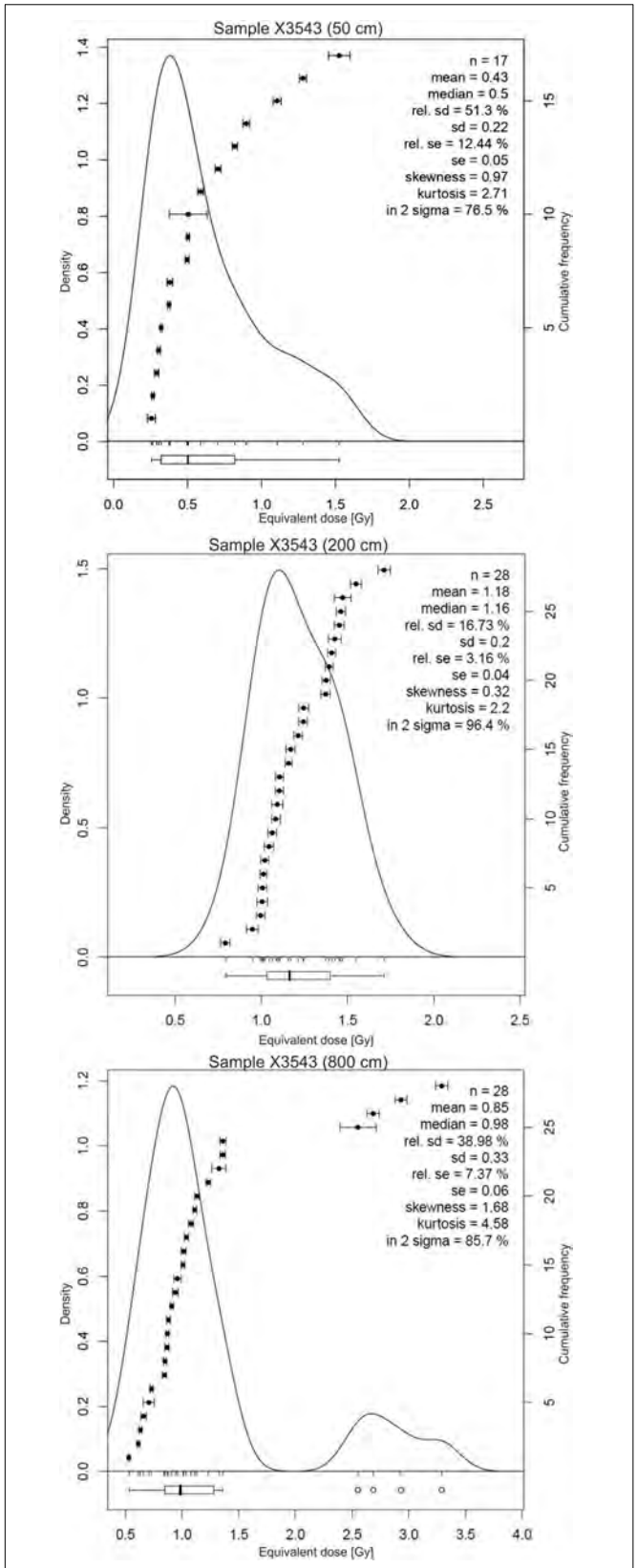


**FIGURE 3 |** Kernel density plots featuring the distribution of individual paleodose values and associated statistical summary for each sample.

**TABLE 3 |** Summary of sub-facies notations, code and their description.

| Sr No | Sediment facies name | Sub-facies code | Sediment facies description |
|---|---|---|---|
| 1. | $Fm_{SILT+VFS(T)}$ | 1 | Massive muddy sub-facies with silt and very fine sand with the presence of foraminifera. |
| 2. | $Fm_{SILT+VFS(O)}$ | 2 | Massive muddy sub-facies, with silt and very fine sand without foraminifera. |
| 3. | $Fm_{SILT+VFS+FS}$ | 3 | Massive muddy sub-facies with silt, very fine sand and fine sand. |
| 4. | $Sl_{FS+VFS}$ | 4 | Laminated sandy facies with fine sand and very fine sand |
| 5. | $Sm_{FS+MS}$ | 5 | Massive sandy facies with fine sand and medium sand |
| 6. | $St_{MS+FS+CS}$ | 6 | Trough cross-bedded sandy facies with medium sand, fine sand and coarse sand |
| 7. | $St_{MS+CS}$ | 7 | Trough cross-bedded sandy facies with medium sand, fine sand and coarse sand |

at 2 cm intervals from 8 m thick sedimentary deposits. High-resolution granulometric data were generated using the sieve and pipette method, and their sedimentological relevance was discussed earlier by Sukumaran et al. (2012b). In the present study, we attempt to integrate granulometric data with other proxies, such as MS and FMC, to determine the tracer capturing the flooding phases.

The description of facies and sub-facies of the Uchediya sediment sequence was decoded using high-resolution granulometric data by applying the cluster analysis method to 14 grain size fractions from 401 samples (Sukumaran et al., 2012b). Each cluster was quantitatively determined, compared, evaluated, and supplemented with field base details to derive the sediment sub-facies. The terminology of the sediment sub-facies was adopted based on the abundance of grain size and primary sedimentary structures in line with lithofacies classification after Miall (1978, 1985) and Martinius (2000). The Uchediya sequence is broadly represented by two facies, viz. sandy facies and muddy facies. The muddy facies are classified into three sub-facies, namely, 1 [$Fm_{SILT+VFS}$ (T)], 2 [Fm $_{SILT+VFS}$ (O)] and 3 ($Fm_{SILT+VFS+FS}$). The sandy facies are further classified into four sub-facies, viz. 4 (Sl $_{FS+VFS}$), 5 (Sm $_{FS+MS}$), 6 (St $_{MS+FS+CS}$), and 7 (St $_{MS+CS}$) (**Table 3** and **Figure 2**).

The sediment facies deduced from high-resolution granulometric data revealed that the Uchediya sediment sequence was aggraded in two distinct phases, namely, aggradation phase I (AP-I) and aggradation phase II (AP-II) (**Figure 4**). AP-I represents a 608 cm thick sandy facies deposited between 194 and 802 cm. The chronological bracket of the sequence suggests that the sequence aggraded in a relatively short period of time. Three distinct sediment sub-facies characterise AP-I. The sub-facies suggest that enough energy conditions were available to mobilise sand viz. channel deposits (couplets of sub-facies 6 and 5 as well as sub-facies 7 and 6) followed by channel margin deposits (sub-facies 4) and transitional deposits (intercalation of sub-facies 2-3-4-5-6; **Figure 2-I**).

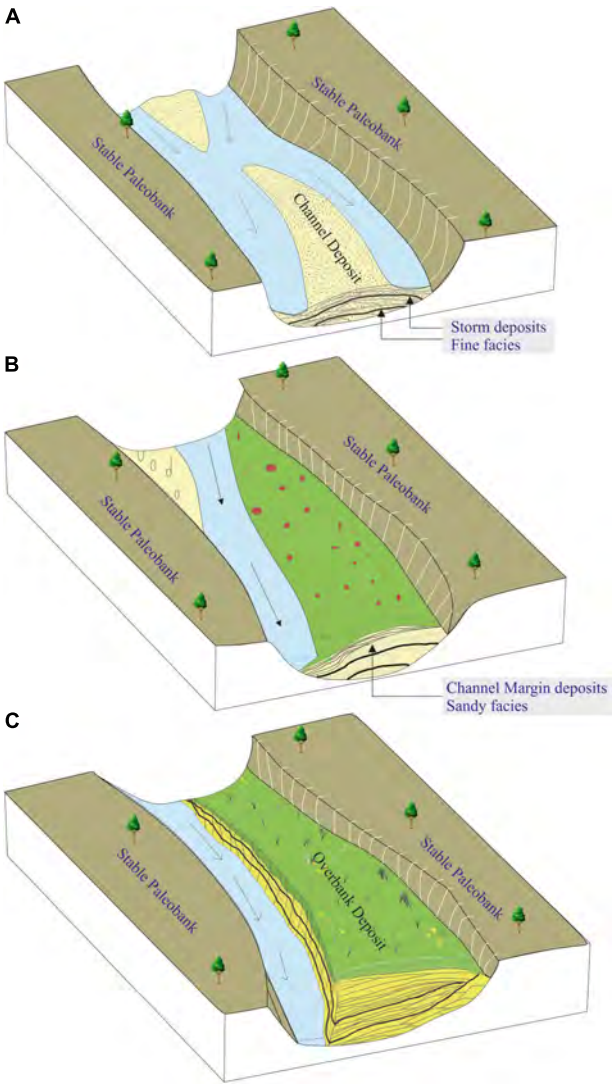


**FIGURE 4 |** A simplified depositional model of Neo-bank development. **(A)** Initiation and aggradation of bar within the channel due to large scale sand movement. **(B)** Stabilisation and merging of the bar with paleobank, sandwiching layers of fine-grained sediments deposited by monsoonal storm deposits, and finally giving way for development of overbank deposits. **(C)** Migration and fixing of the new channel, dominated by bank erosion and down cutting.

Sub-facies 1 are recorded at two depths measured to be from 684 to 638 cm (within two channel facies) and 450–376 cm (within the channel facies to channel margin facies) (**Figure 2-I**). These planktonic microforms bearing unsorted sediments are interpreted as two direct manifestations of monsoonal storms which exerted an influence approximately 56 km inland from the river mouth (Sukumaran et al., 2012a). The evidence of catastrophic storms and channel modifications (change of facies from channel to channel margin and to transition facies) during a brief period of time indicates a changing climate phase in the fluvial archive.

The later phase of sediment aggradation (AP-II) is represented by a 194 cm thick muddy facies (depth from 194 cm to the top of the sequence). The AP II sequence showed distinct disconformity with the underlying AP 1 sequence. The muddy facies are characterised by the intercalation of sub-facies 3 and sub-facies 2, representing overbank deposits (**Figure 2-I**).

## Ferromagnetic Mineral Concentration

Highly magnetic (ferromagnetic) minerals, such as magnetite, are readily separated by the use of a magnet. The ferromagnetic minerals in the present context are the opaque minerals which are naturally magnetic. Primarily such minerals have a very high specific gravity (∼5) compared to the rest of the non-magnetic or paramagnetic minerals in the bulk sediments. Because of their heaviness, they usually travel with light minerals such as quartz averaging 0.5–1.0 phi larger than their size, and they stand as a proxy for hydraulic factors (Folk, 1974). The enrichment or depletion of FMC within the sediment facies is anticipated under two possible conditions: *(i)* the FMCs are mobilised and redistributed in accordance with the energy condition and represented part of the sediment facies; *(ii)* the enrichment of FMC is due to lag, while finer sediments were washed from bulk sediments before the next package of sediment deposited. In either case, FMC remains a part of a sediment facies and represents the fluvial system's energy condition.

FMC is separated from the bulk sediment using a sheath-covered hand-magnet (Rosenblum et al., 2000; Collinson, 2013). A 10 gm of bulk sample was scanned using the hand-magnet and the latter was passed near over such that it did not touch the sample. Several iterations were undertaken to ensure complete extraction. To confirm the effectiveness of the separation, 20 samples were tested with the washing method. The left-out fractions of non-magnetic minerals were transferred to a high-speed stirrer and 50 ml of demineralised water were added and stirred for 10 min. This solution was then stirred for 15 min using a sheath-covered magnetic stirrer. The fraction of FMC attracted to the stirrer was then collected and weighed after drying in a hot air oven. In all the cases, the additional minerals separated from the left-out portion were less than 1.8% of the amount of FMC separated using a hand-magnet. The results of this test confirm the applicability of the adopted method and the obtained results. A total of 205 samples were analysed in this way for the Uchediya sequence. The resolution for the selection of samples for analysis was based on sedimentological inputs. Muddy facies (194 cm from the top of the section) were analysed at 2 cm intervals, whereas sandy facies (196–802 cm) were analysed at 10 cm intervals. The FMC plot against depth differentiates the distribution pattern, capturing three distinct depositional environments: bar sequence, transition sequence, and overbank sequence, suggesting a close relationship of FMC with sediment facies (**Figure 5**).

## Magnetic Susceptibility

As a rapid analytical procedure with a reproducible result, this method has attracted the attention of climate researchers who have used MS as an environmental proxy for the last few decades (Thompson and Morton, 1979; Thompson et al., 1980;

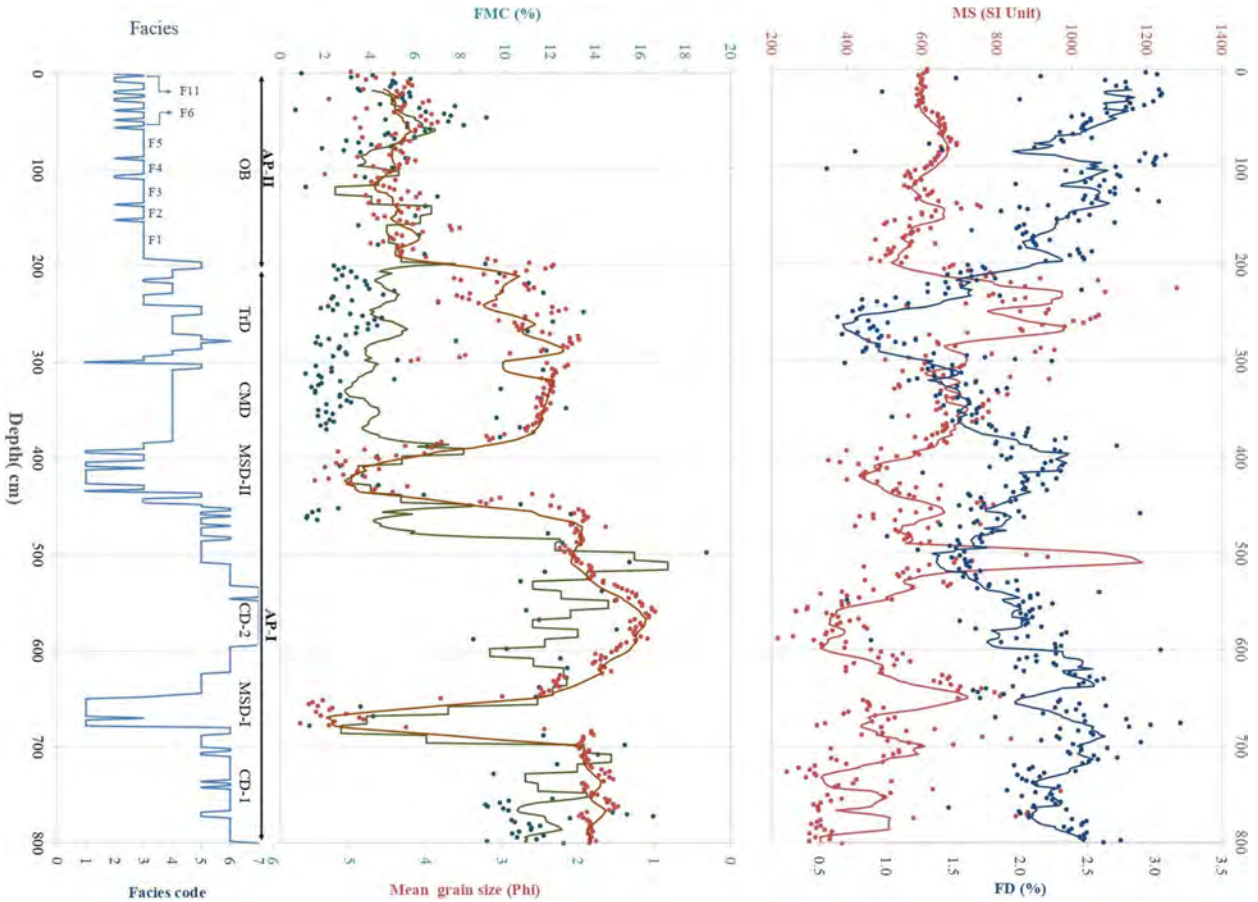


**FIGURE 5 |** Multi-proxy records of the Uchediya section showing depth-wise variation in sediment sub-facies, ferromagnetic mineral concentration (FMC%), mean grain size (Phi), magnetic susceptibility ($\chi_{lf}$) and frequency-dependent susceptibility ($\chi$FD%). The plots distinguish the Aggradation phase I and Aggradation phase II. Aggradation phase I further deciphers Channel Deposit (CD, couplets of 6 and 5 sub-facies and couplets of 6 and 7 sub-facies), Channel Margin Deposits (CMD, sub-facies 4), and Transition Deposit (TrD intercalation of 2, 3, 4, 5, and 6 sub-facies) from 802 to 194 cm. The two phases of monsoonal storms deposits (MSD, sub-facies 1) are conspicuous from 684 to 638 cm (MSD-I) and 450–376 cm (MSD-II) depth. Aggradation phase II highlights overbank deposits (OB, intercalation of 2 and 3 sub-facies) from 194 to 0 cm. F1–F11 indicate inferred flood events.

Heller and Tung-Sheng, 1986; Kukla et al., 1988; Begét et al., 1990; An et al., 1991; Heller et al., 1991; Grimley et al., 1998; Basavaiah and Khadkikar, 2004; Deotare et al., 2004; Rajshekhar et al., 2004; Pant et al., 2005; Pattan et al., 2008; Juyal et al., 2009; Liu et al., 2010). These studies mainly focused on the climate signatures from aeolian sections, paleosols, lacustrine deposits and mudflats, whereas those of fluvial sediments are rarely studied. However, recent investigations have demonstrated that MS can be effectively used as a proxy for high-resolution cross facies correlation in general fluvial systems (Püspöki et al., 2020).

Low field MS was measured on all 401 samples every 2 cm using a multi-functional automated MFK-1 Kapabridge with a sensitivity of $2 \times 10^{-6}$ (SI units). The measurements were done at 976 and 3,904 Hz with a field strength of 133 A/m. The results of the analysis are exhibited in terms of MS and frequency-dependent mineral MS ($\chi$FD%). The frequency effect is usually expressed as a percentage of the MS's difference at lower and high frequencies to the value taken with the lower frequency. MS usually reflects the concentrations of magnetic minerals independent of differences in grain size, while $\chi$FD% is sensitive to the presence of superparamagnetic (SP) particles, which usually are < 100 nm (<0.1μm) in diameter (Dearing et al., 1996; Basavaiah, 2011). Overall, $\chi$FD% values vary from 0.135 to 4.67% for all studied samples. The MS and $\chi$FD% plots along the depth profile differentiate sandy and muddy facies (**Figure 5**). MS represents the contributions from both fine pedogenic particles and coarse detrital sediment input, whereas $\chi$FD% represents the enhancement in the ultrafine magnetic particles during soil formation (Oldfield and Yu, 1994; Basavaiah, 2011).

Together, MS and $\chi$FD% variations, which are anti-correlated, determined the sediment source's signature (**Figure 5**). The sediment sources determine the mineralogy while transport conditions and depositional environments control concentration and grain-size distribution of magnetic minerals. The values of $\chi$FD% of 2.0% indicate virtually no SP grains, between 2.0 and 10.0% they indicate an admixture of SP and coarser non-SP grains, between 10.0 and 14.0% they indicate all SP grains (Dearing et al., 1996; Basavaiah, 2011; Basavaiah et al.,

2015, 2019). Relatively high χFD% values of between 2 and 5% indicate a higher proportion of soil component in a relatively weathered sediment, which is generally characterised by a slower deposition rate. However, low χFD% values < 2% with a higher sedimentation rate indicate freshly derived rock-debris-derived sediment. The MS curve (**Figure 5**) shows marked fluctuations indicating a fluctuating concentration of ferrimagnetic minerals in the sediment input. Generally, higher (or lower) MS values are associated with unaltered (or altered) sediment types during periods of increased (or decreased) sedimentation rates (also evident in anti-correlated χFD% values). Rock magnetic properties help us characterise the type of source responsible for sedimentation (Basavaiah and Khadkikar, 2004; Basavaiah et al., 2010; Basavaiah, 2011; Basavaiah et al., 2019).

## Facies Representative Major Oxide Geochemistry (FMoG)

To assess the possibility of a change in sediment provenance, major element geochemistry was determined from seven distinct sedimentary depositional environments. Each depositional environment was identified and described in terms of sub-facies level well before selecting the samples for analysis (Sukumaran et al., 2012b). The major oxide geochemistry of seven representative samples along the depth profile was studied using ICP AES with a microwave-digested sample, a facility made available by the Department of Earth Sciences at the Indian Institute of Technology in Powai, Mumbai. Major elements such as Al, Fe, Ti, K, Mg, Mn, Na, P, Ca, and Si were quantified and represented as a corresponding oxide weight percentage.

Geochemical records of major elements, namely, Al, Fe, Ti, K, Mg, Mn, Na, P, Ca, and Si, were calculated to their respective oxides. The abundance of oxides representing various depositional environments is tabulated in their percentages (**Table 4**). The correlation matrix of the ten major oxides (**Table 5**) showed that $SiO_2$ (ranging from 62.543 to 84.764%) had a strong negative correlation (−0.9889 to −0.8199 significance) with the other 8 oxides ($Al_2O_3$, $Fe_2O_3$, $TiO_2$, CaO, $Na_2O$, MgO, MnO, and $P_2O_5$). However, $SiO_2$ showed a moderate positive correlation with $K_2O$ (0.558). The correlation matrix further suggested that the oxides, namely $Al_2O_3$, $Fe_2O_3$, $TiO_2$, CaO, $Na_2O$, MgO, MnO, and $P_2O_5$ had mutual strong positive (0.9937–0.66559) correlation, except for $K_2O$, which showed moderate to low negative correlation (−0.6236 to −0.0815) with all other oxides. The present analysis cannot ascertain the $K_2O$ anomaly, and would require a more detailed study at a higher resolution. In other ways, the data indicates a uniformity of sediment source throughout the entire sequence and the variations in composition are only considered to represent selective reworking of hydrodynamic conditions.

# DISCUSSION: INTEGRATION OF PROXY RECORDS

Here, we discuss the interrelationship of the proxies as outlined in the above paragraphs for the 8 m thick sequence at Uchediya. The sediment sequence represents a 45 km long neo-bank on the river Narmada's southern bank in the lower reaches. The interrelationship between proxies enhances the sediment source history, mode of transport and hydrodynamic factors of the SwIM River. We discuss a few scatter plots within the FMoG that provide an overall understanding of sediment uniformity and their source area weathering. The scatter plots between MS, FMC, and granulometric parameters point toward the river system's hydrodynamic conditions during variations in climate in the Holocene. The MS and FMC are mutually dependent variables, where MS is the measure of magnetisable mineral percentage in standard volume, and FMC is the percentage of magnetic minerals in weight percentage. The plot between MS and FMC shows relative density differences between magnetic and non-magnetic minerals, whereas the envelope of sediment sub-facies tends to capture the environment of deposition of these sediments and their hydrodynamics.

**TABLE 4 |** Major elemental geochemistry and CIA of samples.

| Sample no | | UCH 60 | UCH 120 | UCH 160 | UCH 210 | UCH 280 | UCH 330 | UCH 400 |
|---|---|---|---|---|---|---|---|---|
| Depth (cm) | | 120 | 240 | 320 | 420 | 560 | 660 | 800 |
| Facies | | 3 | 3 | 4 | 1 | 7 | 1 | 7 |
| Depositional Environment | | OB | TrD | CMD | MSD-2 | CD | MSD-1 | CD |
| Element (Wt %) | $SiO_2$ | 62.95 | 64.15 | 73.47 | 62.54 | 84.76 | 60.55 | 82.56 |
| | $Al_2O_3$ | 12.87 | 10.06 | 8.25 | 12.65 | 5.29 | 13.28 | 6.17 |
| | $Fe_2O_3$ | 11.20 | 11.07 | 7.25 | 10.48 | 3.20 | 11.15 | 3.74 |
| | CaO | 5.20 | 6.74 | 4.48 | 6.90 | 2.95 | 7.72 | 3.06 |
| | MgO | 2.65 | 2.83 | 2.04 | 2.48 | 0.99 | 2.64 | 1.09 |
| | $TiO_2$ | 2.09 | 2.25 | 1.38 | 1.99 | 0.54 | 1.91 | 0.55 |
| | $Na_2O$ | 1.33 | 1.26 | 1.25 | 1.27 | 0.84 | 1.21 | 1.03 |
| | $K_2O$ | 1.29 | 1.29 | 1.65 | 1.33 | 1.29 | 1.11 | 1.60 |
| | MnO | 0.17 | 0.14 | 0.09 | 0.11 | 0.05 | 0.15 | 0.11 |
| | $P_2O_5$ | 0.13 | 0.13 | 0.11 | 0.13 | 0.06 | 0.14 | 0.08 |
| | LOI | 0.11 | 0.08 | 0.04 | 0.13 | 0.03 | 0.15 | 0.03 |
| | CIA | 62.20 | 52.0 | 52.80 | 57.12 | 51.00 | 56.95 | 52.01 |

**TABLE 5 |** Correlation coefficients of major elemental concentrations.

| | $SiO_2$ | $Al2O_3$ | CaO | $Fe_2O_3$ | $K_2O$ | MgO | MnO | $Na_2O$ | $P_2O_5$ | $TiO_2$ | LOI |
|---|---|---|---|---|---|---|---|---|---|---|---|
| $SiO_2$ | 1.00 | | | | | | | | | | |
| $Al_2\ O_3$ | −0.97 | 1.00 | | | | | | | | | |
| CaO | −0.94 | 0.88 | 1.00 | | | | | | | | |
| $Fe_2O_3$ | −0.99 | 0.94 | 0.91 | 1.00 | | | | | | | |
| $K_2O$ | 0.56 | -0.58 | −0.62 | −0.54 | 1.00 | | | | | | |
| MgO | −0.97 | 0.89 | 0.90 | 0.99 | −0.48 | 1.00 | | | | | |
| MnO | −0.82 | 0.82 | 0.67 | 0.84 | −0.42 | 0.80 | 1.00 | | | | |
| $Na_2O$ | −0.86 | 0.81 | 0.70 | 0.88 | −0.08 | 0.89 | 0.78 | 1.00 | | | |
| $P_2O_5$ | −0.99 | 0.94 | 0.90 | 0.99 | −0.47 | 0.99 | 0.86 | 0.91 | 1.00 | | |
| $TiO_2$ | −0.97 | 0.89 | 0.88 | 0.99 | −0.49 | 0.99 | 0.79 | 0.88 | 0.98 | 1.00 | |
| LOI | −0.91 | 0.96 | 0.89 | 0.87 | −0.72 | 0.80 | 0.75 | 0.64 | 0.86 | 0.79 | 1.00 |

The Uchediya sequence's age bracket falls from 1395 to 1850 AD and coincides with the globally accepted transition phase of the Medieval Warm Period (MWP) to the Little Ice Age (LIA). The LIA is inconsistently defined between a broad time frame of 14th century (AD 1300–1400) and 19th century (AD 1850 and 1900) whereas, the MWP falls ∼1000–1300 AD (Crowley, 2000; Crowley and Lowery, 2000; Mann, 2002; Jones and Mann, 2004). Mostly, the onset of LIA is taken as 1440 AD and ends as late as 1920 AD. The period within the LIA from 1570 to 1750 AD is considered to be the peak phase. Two of the most intense grand solar minima, the Spörer (∼AD 1390–1540) and the Maunder minima (∼ AD 1645–1715) fall within the broader range of LIA (Eddy, 1976; Owens et al., 2017). From the chronology and aggradation model deciphered from the sedimentological analysis, the entire sequence correlates well with the Holocene climate phases. The lower sequence AP-I (CD, CMD, and TrD) preserves the signatures of the waning phase of the MWP, whereas the AP-II (OB) decode the signatures of fluvial responses during the LIA. Considering the LIA phase is said to be globally significant for its socio-cultural and economic impact, and both are associated with manmade and natural calamities (Lamb, 2002; Baker, 2006; Adger et al., 2012), we attempt to establish the interrelationship between various fluvial proxies and understanding sediment transport, distribution, sediment facies and flood events from the Uchediya sequence. Studies from the Paria River basin and the southern Colorado Plateau in the United States have shown that valley-fill alluvium during LIA is a mappable stratigraphic unit within the larger alluvial valley (Hereford, 2002). By contrast, such reports from major SwIM Rivers are sparse.

FMoG reveals the relative variation of sediment geochemistry across the section. The percentage of $SiO_2$ has been plotted against other oxides viz. $Al_2O_3$, $TiO_2$, $Fe_2O_3$, $Na_2O$, CaO, MgO, MnO, and $P_2O_5$ (**Figure 6**). Also, immobile and mobile oxides were plotted against each other viz. $Al_2O_3$ vs. $Fe_2O_3$, $Al_2O_3$ vs. $TiO_2$, $Fe_2O_3$ vs. $TiO_2$, $Na_2O$ vs. $K_2O$, $K_2O$ vs. $P_2O_5$, and CaO vs. $Na_2O$ (**Figure 6**). The scatter plots of various oxides against $SiO_2$ show an inverse relationship. With the decrease in $SiO_2$, the percentage of other oxides also increases, whereas $K_2O$ behaves differently. The various oxides are highest in the facies representing OB, TrD and two storm units (MSD-I and MSD-II). Whereas in the case of CMD and CD, they have a higher percentage of $SiO_2$ than other oxides. $Fe_2O_3$ and $TiO_2$ plotted against $Al_2O_3$ and $TiO_2$ vs. $Fe_2O_3$ show that they increase together and are directly proportional to each other. A distinct position of channel marginal deposits in all the bivariate plots indicates a selective reworking.

Estimating each sample's degree of chemical weathering was obtained by calculating the chemical index of alteration (CIA) (Nesbitt and Young, 1982). Different researchers have extensively used these parameters to understand chemical maturity and provenance weathering (Singh and Rajamani, 2001; Lee et al., 2005; Das and Krishnaswami, 2007; Tripathi et al., 2007; Manikyamba et al., 2008; Oh et al., 2008; Roy et al., 2008; Singh, 2009; Singh, 2010). The CIA values of fresh rocks and minerals are consistently near 50 whereas samples with values below 60 are considered to display low chemical weathering; between 60 and 80, they indicate moderate chemical weathering and values over 80 are seen as exhibiting extreme chemical weathering (Fedo et al., 1995; **Table 4**). The sample (UCH 60) taken from the overbank deposit, indicates moderate chemical weathering (62.20) and further supports the reworking of sediments from older deposits. Simultaneously, lower CIA values recorded from channel deposits, channel margin deposits, and transitional deposits indicate that the sediments are freshly derived from parent rock and reflect a significant fluvial influx.

The plot between MS vs. mean grain size demonstrates two distinct trends clustered by fine and sandy facies (**Figure 7-I**). A positive trend of increase in MS with an increase in mean size is observed in the fine facies that includes sub-facies 1, 2, and 3. In the sand facies, a negative trend is observed in the cluster of sandy facies, which includes sub-facies 4, 5, 6, and 7. The plot of FMC's vs. mean grain size (**Figure 7-II**) demonstrates a uniform trend of MS variation. In both, the fine facies (1, 2, and 3) and the sandy facies (4, 5, 6, and 7), there is a slight increase in FMC with an

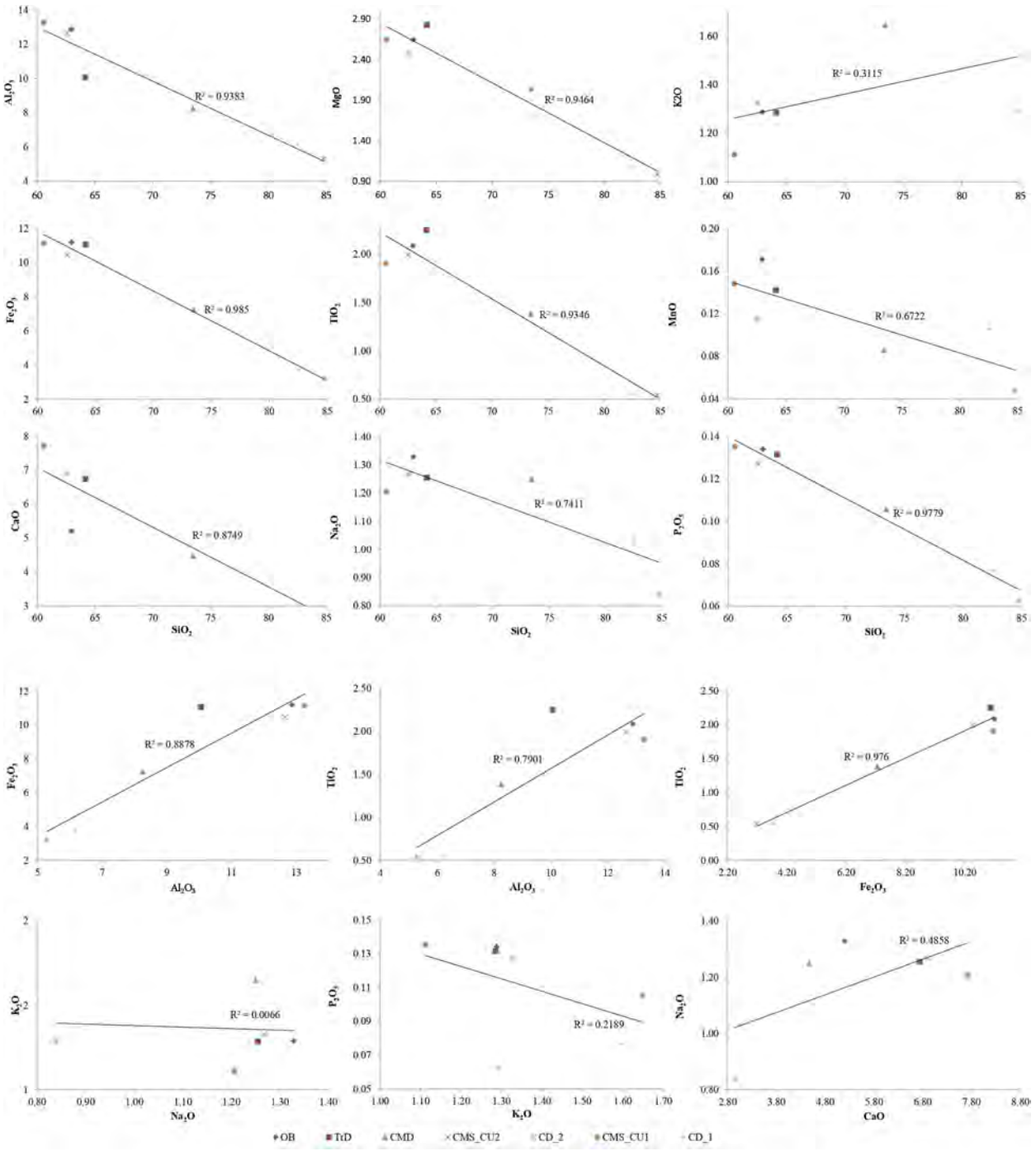


**FIGURE 6 |** Variation diagram of major oxides weight percentage against $SiO_2$ and other oxides.

increase in mean grain size. We consider that the ferromagnetic minerals that travel along with quartz grains would have a relative size variation (an average of 0.5–1.0 phi larger quartz compared to ferromagnetic minerals) due to the heaviness of ferromagnetic minerals (Folk, 1974). Together, MS and FMC may offer the potential to distinguish between alluvium delivered directly from the slopes and material produced by changes in channel morphology. The plot of the ratio of FMC and MS against mean grain size shows a clustering of the sub-facies and a clear trend of variation of the magnetic parameter with mean grain size (**Figure 7-III**). Thus, the relation between FMC and MS appears to establish a sub-facies level interrelationship in recent sediments deposited in a fluvial environment.

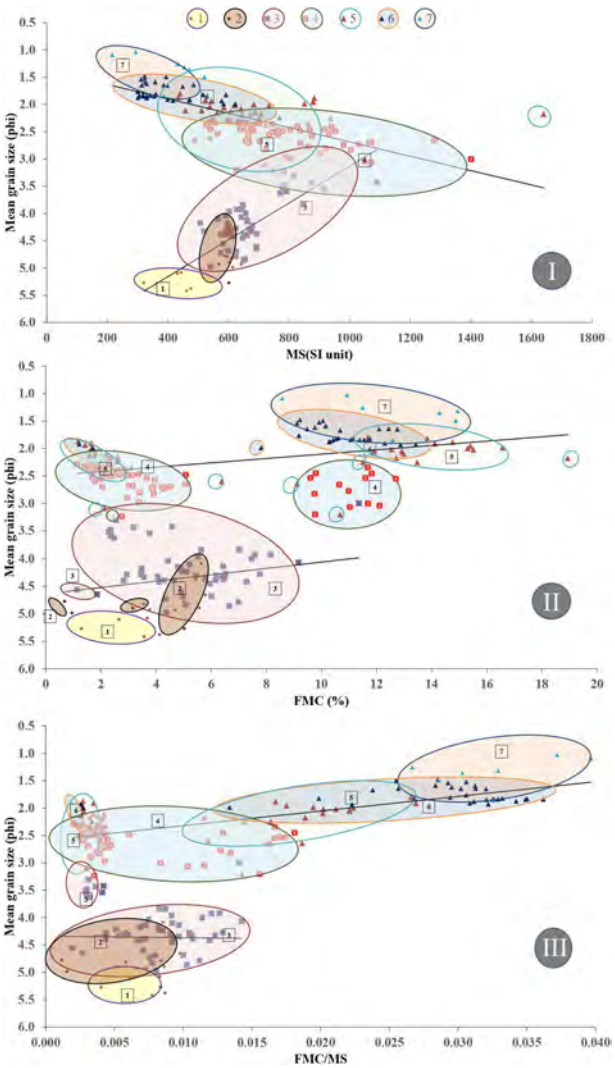


**FIGURE 7 |** Cross plots FMC, MS, and Facies. **(I)** MS vs. Mean grain size showing two distinct trends in fine facies and sandy facies. **(II)** FMC vs. Mean grain size showing two similar trends in fine facies and sandy facies. **(III)** FMC/MS vs. Mean grain size showing two similar trends in fine facies and sandy facies. Coloured circles envelopes similar sediment sub-facies.

The FMC vs. MS scatter-plot demonstrates two clusters roughly demarcated by 8% FMC (**Figure 8**). The cluster of data with more than 8% FMC results from sandy facies, viz. sub-facies 4, 5, 6, and 7. The sub-facies 6, having a higher weight percentage of FMC (8.57–14.94%) but a low MS (216–669 $\times 10^{-6} m^3 kg^{-1}$) may be interpreted as a primary event of sand deposition. Such a situation is possible when the bulk of the sediment contains an abundance of low-density minerals. Sub-facies 7 which is encountered at a depth ranging from 5.34 m to 5.94, is a channel deposit and further supports rapid aggradation and preservation of the sub-facies without any evidence of reworking by the river channel. The other three sandy sub-facies 4, 5, and 6, feature clusterings in excess of 8% FMC as well as minor clustering < 8% FMC. This is likely to be indicative of reworking of channel sand and the three sub-facies are considered to represent channel deposits, channel marginal deposits or transitional deposits.

A second cluster in the FMC vs. MS plot, having less than 8% of FMC and variable MS percentages, includes fine sub-facies, viz. 1, 2, 3, and sandy sub facies viz. 4, 5, and 6. These sandy facies consist of the channel deposit, channel marginal deposits and transitional deposits resulting from the reworking of older deposits. The fine sub-facies, 1 is primarily the result of a tidal influx; the other two fine facies, namely sub facies 2 and 3, are the only sub-facies with distinct depositional characteristics. A specific overlapping and a matching trend of sub-facies 2 and 3 may be interpreted as a characteristic signature of a flood event which was responsible for the deposition of these couplets. Sub-facies 2 and 3 is a primary constituent of the overbank depositional environment, which has preserved at least 11 such couplets that can be interpreted as representing individual flood events (**Figure 5**). The variation of these couplets' thickness may also hint toward the floods' relative energy conditions (Kochel and Baker, 1988). A fundamental reason to consider the flood deposit thickness as a proxy to evaluate the flood energy is the assumption that most other geographic factors remained the same; only the duration of a flood can increase the deposit's thickness. The high-resolution sedimentary record suggests at least five (out of 11) discrete flood events (as the thickness of sediment couplet is between 14 and 40 cm indicating a prolonged submersion of elevated land; F1–F5, **Figure 5**), which had relatively higher energy in comparison with the six flood events (thickness of sediment couplet is between 2 and 8 cm; F6–F11, **Figure 5**). These multiple flood events led to the aggradation of an overbank.

The signatures of climate and flood deciphered from the high-resolution multi-proxy records from the Uchediya sequence help us to compare them with available records of historical flood descriptions from the town of Bharuch which is located on the northern bank of the Narmada River (**Table 6**; Forbes, 1813; Gazetteer, 1961, 1877). One of the factors that may have led to the construction of a fort wall along the Narmada bank in 1094–1143 AD might be related to a past attempt at preventing erosion caused by high energy flow along the northern bank during this period. Rebuilding and strengthening the fort wall during 1526–1536 AD may also testify to the continuation of high energy conditions within the Narmada channel. Until then, the river sustained the passage of large vessels right up to the fort wall. However, a large inflow of sand during 1673–1681 AD led to a shallowing of the channel where vessels with skilled navigators could only reach up to the city walls. Large magnitude flood events were recorded in 1781, 1825, 1835, 1836, 1837, 1860, 1864, 1868, 1870–1877, and 1897 AD, where geomorphic changes such as channel shallowing (1825 AD), the southerly shift of the thalweg line (1860 AD) and erosion of the southern bank (1870–1877 AD) have been documented. Historical evidence such as the rebuilding of the fort wall during the years 1526–1536 AD, the large inflow of sand recorded between 1673 and 1681 AD as well as a shallowing of the river

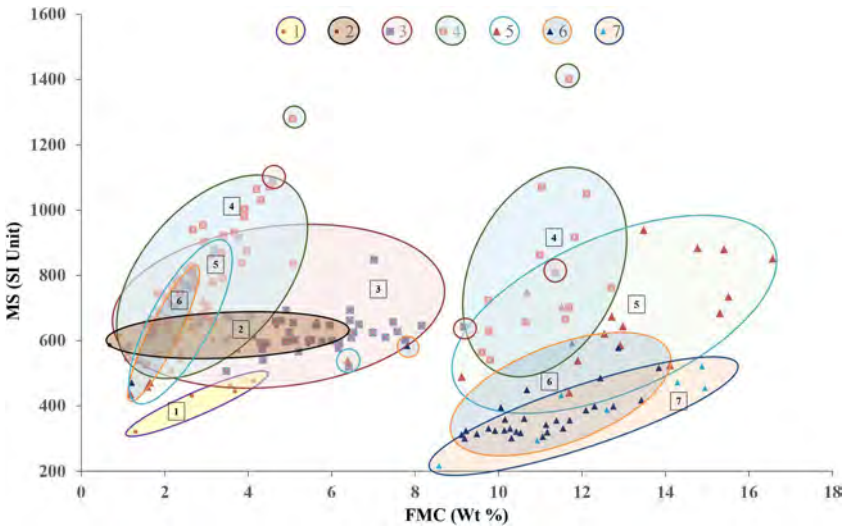


**FIGURE 8 |** The Cross plot of MS vs. FMC shows two groups of clusters roughly demarcated by 8% FMC. < 8% cluster includes sub-facies 1–6 and > 8% cluster includes sub-facies 4–7. The fine sub-facies, 1 is distinct and belongs to tidal influx; the other two fine sub facies 2 and 3 are a primary constituent of the overbank deposits. The overlapping/matching trend of sub-facies 2 and 3, therefore, considered capturing facies-couplets representing flood events.

**TABLE 6 |** Historical records documented for Bharuch town with respect to changes in the Narmada River.

| Period | Description |
|---|---|
| 1094–1143 | The archaeological structure, Fort Wall built on the right bank of Narmada to prevent the city from erosion was built by Sidh Raj Jaisinhji of Anhilwara during 1094–1143 (Bombay presidency gazetteer 1877–1905, p. 551). |
| 1526–1536 | Bahadur Shah strengthened and rebuilt the Fort wall. This is also noted that the large ships were reaching up to the city wall during the period (Bombay presidency gazetteer 1877–1905, p. 55). |
| *1673–1681* | *-Two hundred years ago when Fryer (1673–1681) crossed the river at Broach, he found the stream broad, swift and deep, but adds that, on account of the sand forced down to the rain skilful pilots are required, by whose direction good lusty vessels are brought up to the city walls* (Bombay presidency gazetteer 1877–1905). |
| *1781* | A storm passed over the district of Bharuch, of which Mr. Forbes has left an account in the Oriental memories- Forbes Oriental Memoirs, vol-III, 53. *"Two years before I left India, some weeks before the setting into the south-west monsoon (May), we had the most deadly storm ever remembered in Gujarat. It ravage by sea and land were terrible, the damage at Broch was very great, and the loss of life considerable".* |
| *1822* | *Large flood (*Kale et al., 1997a*).* |
| *1825* | *-Bishop Herber (1825) visited Broch, he noticed that the Narmada was very shallow and that then no vessel larger than moderately sized lighters could come beyond the bar.* (Bombay presidency gazetteer 1877–1905). |
| 1835 | Cold environment (Gazetteer, 1961, p. 303). |
| 1836 | Heavy rain (Gazetteer, 1961, p. 303). |
| 1837 | *-Great flood-1937, when the water of Narbada and Tapi are said to be have joined. No damage would seem to have been caused either to the district or the city of Broch it has not done much damage to the Broach city* (Gazetteer, 1877, page 410). |
| *1838* | Failure of Rain (Gazetteer, 1961, p. 303). |
| *1840* | Failure of Rain (Gazetteer, 1961, p. 303). |
| *1860* | Nineteenth century story of Narmada was much devastating. *-At the time when the original bridge was built the heavy current of the stream lays on the right bank. Since then the main channel of the river has so entirely shifted toward the left bank* (Bombay Presidency Gazetteer of the year 1877-1905 is about the built of Golden bridge; from page 419 and 420). |
| *1864* | *- A flood rising within 21 feet rail level carried away six spans in the deep water channel* (Bombay Presidency Gazetteer of year 1877–1905 is about the built of Golden bridge; from page 419 and 420). |
| *1868* | *-August flood rising to 18 feet of rail level carried away four spans* (Bombay Presidency Gazetteer of the year 1877–1905 is about the built of Golden bridge; from page 419 and 420). |
| 1870–1877 | *-During 7 years the southern bank was gradually washed away, and driven back upward of 1000 feet.* (Bombay Presidency Gazetteer of the year 1877–1905 is about the built of Golden bridge; from page 419 and 420). |
| *1878* | *Large flood* (Kale et al., 1997a). |
| *1891* | *Large flood* (Kale et al., 1997a). |
| *1894* | *Large flood* (Kale et al., 1997a). |
| *1897* | *-The water rising suddenly to the unprecedented height of 35 feet above high water mark or within 13'6" of rail level, washed away twenty-six spans or upwards of 1600 feet of the southern portion of the bridge.* (Bombay Presidency Gazetteer of the year 1877–1905 is about the built of Golden bridge; from page 419 and 420). |

channel lend additional support to the inferences made from the multi-proxy fluvial record.

## CONCLUSION

- A multi-proxy high-resolution record proposed a stage-wise aggradation history of the neo-bank sedimentary sequence. Rapid aggradation of channel sediments and tidal surges occurred during the initiation of channel modifications and are capped by an overlying 2 m thick overbank deposit.
- A fresh deposit of sandy sediment, frequent channel modifications and high energy conditions close to the $565 \pm 60$ years before 2020 was broadly interpreted as the signature for the MWP waning phase and the onset of the LIA in a SwIM river in western India.
- A couplet of sub-facies 2 ($Fm_{SILT+VFS}$ (O) and 3 ($Fm_{SILT+VFS+FS}$) of overbank deposits were inferred as a signature of past flood events.
- Multi-proxy records enabled to identify signatures of at least 11 distinct flood events within the overbank sediment sequence during a time frame of 500 years.
- MS is a potential proxy to distinguish between sediment delivered directly from the slopes and reworked sediment deposited due to changes in channel morphology. Higher MS and lower $\chi$FD% in coarser unaltered sediments reflect high stream energies and episodes of accelerated delivery of ferrimagnetic minerals of primary origin.
- FMC and MS were effectively utilised as proxies capturing the hydrodynamic conditions of the fluvial system. More such studies from varied depositional environments might help to derive an empirical relationship between FMC, MS, and other granulometric parameters that effectively correlate to past climatic and associated hydrodynamic conditions.
- The study is a step forward toward building a high resolution, multi-proxy sediment archive of monsoonal rivers.

## DATA AVAILABILITY STATEMENT

The raw data supporting the conclusions of this article will be made available by the authors, without undue reservation.

## AUTHOR CONTRIBUTIONS

PS worked for his Ph.D. thesis taking this as study area. DS guided PS throughout his research and contributed in all aspects of the research. KK and GR were co-investigators on the project and participated in the collection of samples, the analysis of data, and the interpretation of results. NB contributed toward magnetic study and interpretation of the results. J-LS carried out the luminescence dating. All authors contributed to the article and approved the submitted version.

## FUNDING

The present work was carried out with project grant from Department of Science and Technology, India under Shallow Sub-surface Science Program, Narmada Window (SR/S4/ES-21/NARMADA WINDOW/P 6). GR was also supported by the J. C. Bose National Fellowship and UGC Center for Advanced Studies.

## ACKNOWLEDGMENTS

We thank the Department of Earth Sciences, Indian Institute of Technology, Powai, Mumbai, for extending the ICP AES, facility. We thank Professor Mark Maslin, Department of Geography, University College London, and Prof. Robert J. Wasson, Emeritus Professor at the Australian National University for reviewing and suggesting modifications to the manuscript and figures. PS is thankful to Dr. Hiteshri Shastri for sharing the hydro-climatology laboratory facility for the geospatial analysis. A critical review and suggestions by two reviewers have substantially improved the manuscript in many aspects.

## REFERENCES

Adger, W. N., Kelly, P. M., and Ninh, N. H. (2012). *Living with Environmental Change: Social Vulnerability, Adaptation and Resilience in Vietnam*. London: Routledge.

Aitken, M. J. (1998). *An Introduction to Optical Dating*. Oxford: Oxford University Press.

An, Z., Kukla, S., Porter, S. C., and Xiao, J. L. (1991). Magnetic susceptibility evidence of monsoon variation on the Loess Plateau of Central China during the last 13 000 years. *Quat. Res.* 36, 29–36. doi: 10.1016/0033-5894(91)90015-w

Baker, V. (1995). Global paleohydrological change. *Quaestiones Geogr.* 4, 27–35.

Baker, V. R. (2006). Palaeoflood hydrology in a global context. *Catena* 66, 161–168. doi: 10.1016/j.catena.2005.11.016

Banerjee, D., Murray, A. S., Bøtter-Jensen, L., and Lang, A. (2001). Equivalent dose estimation using a single aliquot of polymineral fine grains. *Radiat. Meas.* 33, 73–94. doi: 10.1016/s1350-4487(00)00101-3

Basavaiah, N. (2011). *Geomagnetism: Solid Earth and Upper Atmosphere Perspectives*. Dordrecht: Springer.

Basavaiah, N., Appel, E., Lakshmi, B. V., Deenadayalan, K., Satyanarayana, K. V. V., Misra, S., et al. (2010). Revised magnetostratigraphy and nature of the fluvio-lacustrine sedimentation of the Kashmir basin, India, during Pliocene-Pleistocene. *J. Geophys. Res.* 115: B08105.

Basavaiah, N., Babu, J. M., Gawali, P., Kumar, K. C. V. N., Demudu, G., Prizomwala, S. P., et al. (2015). Late quaternary environmental and sea level changes from Kolleru Lake, SE India: inferences from mineral magnetic, geochemical and textural analyses. *Quat. Int.* 371, 197–208. doi: 10.1016/j.quaint.2014.12.018

Basavaiah, N., Babu, J. M., Prizomwala, S., Achyuthan, H., Siva, V., and Boral, P. (2019). Proxy mineral magnetic and elemental analyses for 2004 tsunami impact deposit along the Muttukadu backwater, East Coast of India: scope of the palaeotsunami studies. *Quat. Int.* 507, 224–232. doi: 10.1016/j.quaint.2018.10.038

Basavaiah, N., and Khadkikar, A. S. (2004). Environmental magnetism and it s application towards palaeomonsoon reconstruction. *J. Indian Geophys. Union* 8, 1–14.

Bedi, N., and Vaidyanadhan, R. (1982). Effect of neotectonics on the morphology of the Narmada river in Gujarat, Western India *Z.Geomorph.N.F*, 87–102.

Begét, J. E., Stone, D. B., and Hawkins, D. B. (1990). Paleoclimatic forcing of magnetic susceptibility variations in Alaskan loess during the late Quaternary. *Geology* 18, 40–43. doi: 10.1130/0091-7613(1990)018<0040:pfomsv>2.3.co;2

Bøtter-Jensen, L. (1997). Luminescence techniques: instrumentation and methods. *Radiat. Meas.* 27, 749–768. doi: 10.1016/s1350-4487(97)00206-0

Chamyal, L. S., Maurya, D. M., Bhandari, S., and Raj, R. (2002). Late quaternary geomorphic evolution of the lower Narmada valley, Western India: implications for neotectonic activity along the Narmada-Son Fault. *Geomorphology* 46, 177–202. doi: 10.1016/s0169-555x(02)00073-9

Collinson, D. (2013). *Methods in Rock Magnetism and Palaeomagnetism: Techniques and Instrumentation*. Berlin: Springer Science & Business Media.

Crowley, T. J. (2000). Causes of climate change over the past 1000 years. *Science* 289, 270–277. doi: 10.1126/science.289.5477.270

Crowley, T. J., and Lowery, T. S. (2000). How warm was the medieval warm period? *AMBIO J. Hum. Environ.* 29, 51–54. doi: 10.1579/0044-7447-29.1.51

Das, A., and Krishnaswami, S. (2007). Elemental geochemistry of river sediments from the Deccan Traps, India: implications to sources of elements and their mobility during basalt–water interaction. *Chem. Geol.* 242, 232–254. doi: 10.1016/j.chemgeo.2007.03.023

Dearing, J. A., Dann, R., Hay, K., Lees, J., Loveland, P., Maher, B. A., et al. (1996). Frequency-dependent susceptibility measurements of environmental materials. *Geophys. J. Int.* 124, 228–240. doi: 10.1111/j.1365-246x.1996.tb06366.x

Deotare, B., Kajale, M., Rajaguru, S., and Basavaiah, N. (2004). Late quaternary geomorphology, palynology and magnetic susceptibility of playas in western margin of the Indian Thar Desert. *Indian Geophys. Union* 8, 15–25.

Duller, G. (2015). The Analyst software package for luminescence data: overview and recent improvements. *Anc. TL* 33, 35–42.

Durcan, J. A., King, G. E., and Duller, G. A. (2015). DRAC: dose rate and age calculator for trapped charge dating. *Quat. Geochronol.* 28, 54–61. doi: 10.1016/j.quageo.2015.03.012

Eddy, J. A. (1976). The maunder minimum. *Science* 192, 1189–1202.

Ely, L. L., Enzel, Y., Baker, V. R., Kale, V. S., and Mishra, S. (1996). Changes in the magnitude and frequency of late holocene monsoon floods on the Narmada River, central India. *Geol. Soc. Am. Bull.* 108, 1134–1148. doi: 10.1130/0016-7606(1996)108<1134:citmaf>2.3.co;2

Fedo, C. M., Wayne Nesbitt, H., and Young, G. M. (1995). Unraveling the effects of potassium metasomatism in sedimentary rocks and paleosols, with implications for paleoweathering conditions and provenance. *Geology* 23, 921–924. doi: 10.1130/0091-7613(1995)023<0921:uteopm>2.3.co;2

Folk, R. L. (1974). *Petrology of Sedimentary Rocks*. Austin, TX: Hemphil Publishing Company.

Forbes, J. (1813). *Oriental Memoirs*. White, Cochrane, and Co: London.

Gao, H., Li, Z., Pan, B., Liu, F., and Liu, X. (2016). Fluvial responses to late quaternary climate change in the Shiyang River drainage system, western China. *Geomorphology* 258, 82–94. doi: 10.1016/j.geomorph.2016.01.018

Gazetteer, B. P. (1877). *Bombay Presidency Gazetteer*. Broch dist.

Gazetteer, B. P. (1961). *Bombay Presidency Gazetteer 1877–1905*. Government Central Press, Bombay.

Grimley, D. A., Follmer, L. R., and Mckay, E. D. (1998). Magnetic susceptibility and mineral zonations controlled by provenance in loess along the Illinois and Central Mississippi River Valleys. *Quat. Res.* 49, 24–36. doi: 10.1006/qres.1997.1947

Guérin, G., Mercier, N., and Adamiec, G. (2011). Dose-rate conversion factors: update. *Anc. TL* 29, 5–8.

Hansen, V., Murray, A., Buylaert, J.-P., Yeo, E.-Y., and Thomsen, K. (2015). A new irradiated quartz for beta source calibration. *Radiat. Meas.* 81, 123–127. doi: 10.1016/j.radmeas.2015.02.017

Heller, F., Liu, X., Liu, T., and Xu, T. (1991). Magnetic susceptibility of loess in China. *Earth Planet. Sci. Lett.* 103, 301–310. doi: 10.1016/0012-821x(91)90168-h

Heller, F., and Tung-Sheng, L. (1986). Palaeoclimatic and sedimentary history from magnetic susceptibility of loess in China. *Geophys. Res. Lett.* 13, 1169–1172. doi: 10.1029/gl013i011p01169

Hereford, R. (2002). Valley-fill alluviation during the Little Ice Age (ca. A.D. 1400–1880), Paria River basin and southern Colorado Plateau, United States. *GSA Bull.* 114, 1550–1563. doi: 10.1130/0016-7606(2002)114<1550:vfadtl>2.0.co;2

Jones, P. D., and Mann, M. E. (2004). Climate over past millennia. *Rev. Geophys.* 42:RG2002.

Joshi, P. N., Maurya, D. M., and Chamyal, L. S. (2013). Tectonic and climatic controls on late Quaternary bajada sedimentation along Narmada-Son Fault (NSF), Gujarat, Western India. *Int. J. Sediment Res.* 28, 66–76. doi: 10.1016/s1001-6279(13)60019-0

Juyal, N., Pant, R. K., Basavaiah, N., Bhushan, R., Jain, M., Saini, N. K., et al. (2009). Reconstruction of last glacial to early Holocene monsoon variability from relict lake sediments of the Higher Central Himalaya, Uttrakhand, India. *J. Asian Earth Sci.* 34, 437–449. doi: 10.1016/j.jseaes.2008.07.007

Kale, V., Achyuthan, H., Jaiswal, M., and Sengupta, S. (2010). Palaeoflood records from upper Kaveri River, southern India: evidence for discrete floods during Holocene. *Geochronometria* 37, 49–55. doi: 10.2478/v10003-010-0026-0

Kale, V. S., and Baker, V. R. (2006). An extraordinary period of low-magnitude floods coinciding with the Little Ice Age: palaeoflood evidence from Central and Western India. *J. Geol. Soc. India* 68, 477–483.

Kale, V. S., Hire, P., and Baker, V. R. (1997a). Flood hydrology and geomorphology of monsoon-dominated rivers: the Indian Peninsula. *Water Int.* 22, 259–265. doi: 10.1080/02508069708686717

Kale, V. S., Mishra, S., and Baker, V. (1997b). A 2000-year palaeoflood record from Sakarghat on Narmada, Central India. *J. Geol. Soc. India* 50, 283–288.

Kale, V. S., Mishra, S., and Baker, V. R. (2003). Sedimentary records of palaeofloods in the bedrock gorges of the Tapi and Narmada rivers, central India. *Curr. Sci.* 84, 1072–1079.

Kochel, R. C., and Baker, V. R. (1988). "Palaeoflood analysis using slackwater deposits," in *Flood Geomorphology*, eds V. R. Baker, R. C. Kochel, and P. C. Patton (New York, NY: John Wiley), 357–376.

Kolb, T., Fuchs, M., and Zöller, L. (2016). Deciphering fluvial landscape evolution by luminescence dating of river terrace formation: a case study from Northern Bavaria, Germany. *Z. Geomorphol.* 60, 29–48. doi: 10.1127/zfg_suppl/2015/s-00193

Kreutzer, S., Schmidt, C., Fuchs, M. C., Dietze, M., Fischer, M., and Fuchs, M. (2012). Introducing an R package for luminescence dating analysis. *Anc. TL* 30, 1–8. doi: 10.1007/978-94-007-6326-5_121-2

Kukla, G., Heller, F., Ming, L. X., Chun, X. T., Sheng, L. T., and Sheng, A. Z. (1988). Pleistocene climates in China dated by magnetic susceptibility. *Geology* 16, 811–814. doi: 10.1130/0091-7613(1988)016<0811:pcicdb>2.3.co;2

Lamb, H. H. (2002). *Climate, History and the Modern World*. Abingdon: Taylor & Francis.

Lee, J. I., Park, B. K., Jwa, Y. J., Yoon, H. I., Yoo, K. C., and Kim, Y. (2005). Geochemical characteristics and the provenance of sediments in the Bransfield Strait, West Antarctica. *Mar. Geol.* 219, 81–98. doi: 10.1016/j.margeo.2005.06.002

Liu, J., Chen, Z., Chen, M., Yan, W., Xiang, R., and Tang, X. (2010). Magnetic susceptibility variations and provenance of surface sediments in the South China Sea. *Sediment. Geol.* 230, 77–85. doi: 10.1016/j.sedgeo.2010.07.001

Manikyamba, C., Kerrich, R., González–Lvarez, I., Mathur, R., and Khanna, T. C. (2008). Geochemistry of Paleoproterozoic black shales from the Intracontinental Cuddapah basin, India: implications for provenance, tectonic setting, and weathering intensity. *Precambrian Res.* 162, 424–440. doi: 10.1016/j.precamres.2007.10.003

Mann, M. E. (2002). "Little ice age," *Encyclopedia of Global Environmental Change*, Vol. 1, eds M. C. MacCracken, and J. S. Perry (Chichester: Wiley), 504–509.

Martinius, A. W. (2000). Labyrinthine facies architecture of the Tortola Fluvial system and controls on deposition (late Oligocene-Early Miocene, Loranca Basin, Spain). *J. Sediment. Res.* 70, 850–867. doi: 10.1306/2dc4093d-0e47-11d7-8643000102c1865d

Miall, A. D. (1978). Lithofacies types and vertical profile models in braided river deposits: a summary. *Fluvial Sedimentol.* 5, 597–604.

Miall, A. D. (1985). Architectural-element analysis: a new method of facies analysis applied to fluvial deposits. *Earth Sci. Rev.* 22, 261–308. doi: 10.1016/0012-8252(85)90001-7

Murray, A. S., and Wintle, A. G. (2000). Luminescence dating of quartz using an improved single-aliquot regenerative-dose protocol. *Radiat. Meas.* 32, 57–73. doi: 10.1016/s1350-4487(99)00253-x

Nesbitt, H. W., and Young, G. M. (1982). Early Proterozoic climates and plate motions inferred from major element chemistry of lutites. *Nature* 299, 715–717. doi: 10.1038/299715a0

Oh, K.-C., Kim, J.-Y., Yang, D.-Y., Lee, J.-Y., and Hong, S.-S. (2008). An assessment of the sand resources in old riverbeds and flood plain deposits within a branch

of the Geum River, South Korea. *Quat. Int.* 176-177, 156–171. doi: 10.1016/j.quaint.2007.06.003

Oldfield, F., and Yu, L. (1994). The influence of particle size variations on the magnetic properties of sediments from the north-eastern Irish Sea. *Sedimentology* 41, 1093–1108. doi: 10.1111/j.1365-3091.1994.tb01443.x

Owens, M. J., Lockwood, M., Hawkins, E., Usoskin, I., Jones, G. S., Barnard, L., et al. (2017). The Maunder minimum and the Little Ice Age: an update from recent reconstructions and climate simulations. *J. Space Weather Space Clim.* 7:A33.

Pant, R. K., Basavaiah, N., Juyal, N., Saini, N. K., Yadava, M. G., Appel, E., et al. (2005). A 20−ka climate record from Central Himalayan loess deposits. *J. Quat. Sci.* 20, 485–492. doi: 10.1002/jqs.938

Pattan, J. N., Parthiban, G., Banakar, V. K., Tomer, A., and Kulkarni, M. (2008). Relationship between chemical composition and magnetic susceptibility in sediment cores from Central Indian Ocean Basin. *J. Earth Syst. Sci.* 117, 113–119. doi: 10.1007/s12040-008-0002-5

Prescott, J. R., and Hutton, J. T. (1994). Cosmic ray contributions to dose rates for luminescence and ESR dating: large depths and long-term time variations. *Radiat. Meas.* 23, 497–500. doi: 10.1016/1350-4487(94)90086-8

Püspöki, Z., Fogarassy-Pummer, T., Thamó-Bozsó, E., Berényi, B., Cserkész-Nagy, Á, Szappanos, B., et al. (2020). High-resolution stratigraphy of a Quaternary fluvial deposit based on magnetic susceptibility variations (Jászság Basin, Hungary). *Boreas* 49, 181–199. doi: 10.1111/bor.12412

Raj, R. (2008). Occurrence of volcanic ash in the Quaternary alluvial deposits, lower Narmada basin, western India. *J. Earth Syst. Sci.* 117, 41–48. doi: 10.1007/s12040-008-0011-4

Raj, R., and Yadava, M. G. (2009). Late Holocene uplift in the lower Narmada basin, western India. *Curr. Sci.* 96, 985–988.

Rajshekhar, C., Gawali, P., Mudgal, T., Reddy, P., and Basavaiah, N. (1991). Micropaleontology and mineral magnetic evidences of the Holocene mudflats of Navlakhi, Gulf of Kachchh. *J. Ind. Geophys. Union* 8, 71–77.

Rajshekhar, C., Gawali, P. B., Mudgal, T. R., Reddy, P. P., and Basavaiah, N. (2004). Micropaleontology and mineral magnetic evidences of the Holocene mudflats of Navlakhi, Gulf of Kuchchh. *J. Ind. Geophys. Union* 8, 71–77.

Rosenblum, S., Leo, G. W., and Srivastava, S. P. (2000). *Methods and Preliminary Results of Heavy-Mineral Studies in Liberia*. Denver, CO: US Department of the Interior, US Geological Survey.

Roy, P. D., Caballero, M., Lozano, R., and Smykatz-Kloss, W. (2008). Geochemistry of late quaternary sediments from Tecocomulco lake, central Mexico: implication to chemical weathering and provenance. *Chem. Erde Geochem.* 68, 383–393. doi: 10.1016/j.chemer.2008.04.001

Sant, D. A., and Karanth, R. V. (1993). Drainage evolution of the lower Narmada valley, western India. *Geomorphology* 8, 221–244.

Singh, P. (2009). Major, trace and REE geochemistry of the Ganga River sediments: influence of provenance and sedimentary processes. *Chem. Geol.* 266, 251–264.

Singh, P. (2010). Geochemistry and provenance of stream sediments of the Ganga River and its major tributaries in the Himalayan region, India. *Chem. Geol.* 269, 220–236. doi: 10.1016/j.chemgeo.2009.09.020

Singh, P., and Rajamani, V. (2001). Geochemistry of the floodplain sediments of the Kaveri River, Southern India. *J. Sediment. Res.* 71, 50–60. doi: 10.1306/042800710050

Sridhar, A., Bhushan, R., Balaji, D., Band, S., and Chamyal, L. S. (2016). Geochemical and Sr–Nd isotopic variations in palaeoflood deposits at mainstem–tributary junction, western India: implications on late Holocene flood events. *Catena* 139, 32–43. doi: 10.1016/j.catena.2015.12.004

Sridhar, A., and Chamyal, L. S. (2010). Sediment records as archives of the Late Pleistocene-Holocene hydrological change in the alluvial Narmada River basin, western India. *Proc. Geol. Assoc.* 121, 195–202. doi: 10.1016/j.pgeola.2010.01.001

Sridhar, A., Laskar, A., Prasad, V., Sharma, A., Tripathi, J. K., Balaji, D., et al. (2015). Late Holocene flooding history of a tropical river in western India in response to southwest monsoon fluctuations: a multi proxy study from lower Narmada valley. *Quat. Int.* 371, 181–190.

Sridhar, A., Thakur, B., Basavaiah, N., Seth, P., Tiwari, P., and Chamyal, L. (2020). Lacustrine record of high magnitude flood events and climate variability during mid to late Holocene in the semiarid alluvial plains, western India. *Palaeogeogr. Palaeoclimatol. Palaeoecol.* 542:109581.

Stanford, S. D., Witte, R. W., Braun, D. D., and Ridge, J. C. (2016). Quaternary fluvial history of the Delaware River, New Jersey and Pennsylvania, USA: the effects of glaciation, glacioisostasy, and eustasy on a proglacial river system. *Geomorphology* 264, 12–28.

Sukumaran, P., Rajshekhar, C., Sant, D. A., and Krishnan, K. (2012a). Late holocene storm records from lower reaches of Narmada Valley, western India. *J. Geol. Soc. India* 80, 403–408.

Sukumaran, P., Sant, D. A., Krishnan, K., and Rangarajan, G. (2012b). High resolution facies record on late holocene flood plain sediments from lower reaches of Narmada Valley, Western India. *J. Geol. Soc. India* 79, 41–52.

Sun, X., Li, Y., Feng, X., Lu, C., Lu, H., Yi, S., et al. (2016). Pedostratigraphy of aeolian deposition near the Yunxian Man site on the Hanjiang River terraces, Yunxian Basin, central China. *Quat. Int.* 400, 187–194.

Thomas, P. J., Juyal, N., Kale, V. S., and Singhvi, A. K. (2007). Luminescence chronology of late Holocene extreme hydrological events in the upper Penner River basin, South India. *J. Quat. Sci.* 22, 747–753.

Thompson, R., and Morton, D. (1979). Magnetic susceptibility and particle size distribution in recent sediments of the Loch Lomond drainage basin, Scotland. *J. Sediment. Petrol.* 49, 0801–0812.

Thompson, R., Stober, J., Turner, G., Oldfield, F., Bloemendal, J., Dearing, J., et al. (1980). Environmental applications of magnetic measurements. *Science* 207, 481–486.

Tripathi, J. K., Ghazanfari, P., Rajamani, V., and Tandon, S. K. (2007). Geochemistry of sediments of the Ganges alluvial plains: evidence of large-scale sediment recycling. *Quat. Int.* 159, 119–130.

Vázquez, G., Solís, B., Solleiro-Rebolledo, E., and Goguitchaichvili, A. (2016). Mineral magnetic properties of an alluvial paleosol sequence in the Maya Lowlands: late Pleistocene–Holocene paleoclimatic implications. *Quat. Int.* 418, 10–21.

**Conflict of Interest:** The authors declare that the research was conducted in the absence of any commercial or financial relationships that could be construed as a potential conflict of interest.